

Femtosecond torsional relaxation

J. Clark^{1*}, T. Nelson², S. Tretiak², G. Cirimi³ and G. Lanzani^{4,5}

Molecular conformational reorganization following photon absorption is a fundamental process driving reactions such as the *cis-trans* isomerization at the heart of the primary step of vision and can be exploited for switching in artificial systems using photochromics. In general, conformational change occurs on a timescale defined by the energy of the main vibrational mode and the rate of energy dissipation. Typically, for a conformational change such as a twist around the backbone of a conjugated molecule, this occurs on the tens of picoseconds timescale. However, here we demonstrate experimentally that in certain circumstances the molecule, in this case an oligofluorene, can change conformation over two orders of magnitude faster (that is sub-100 fs) in a manner analogous to inertial solvent reorganization demonstrated in the 1990s. Theoretical simulations demonstrate that non-adiabatic transitions during internal conversion can efficiently convert electronic potential energy into torsional kinetic energy, providing the 'kick' that prompts sub-100 fs torsional reorganization.

We discovered the phenomenon of femtosecond torsional reorganization in oligofluorenes, a subset of a broad class of conjugated materials that are widely studied for their intriguing photophysics as well as for applications in photonic^{1–5}, light-emitting^{6,7} and photovoltaic devices^{8,9}. A characteristic of these systems is the torsional dynamics about the conjugated backbone that can have a pronounced effect on device physics and spectroscopy^{10,11}. In solution, the inter-ring dihedral angle modulates π -electron delocalization and affects the molecular relaxation paths. Similar torsional motion is at the root of isomerization of molecules such as retinal, found in the eye¹², or azobenzene, a common photochromic material¹³. In general, following photoexcitation, the molecular conformation relaxes towards a new equilibrium geometry^{14,15} typically on a tens of picoseconds timescale^{12,13,16–21}. Here we demonstrate that in oligofluorenes in solution, we can speed up the torsional relaxation from ~ 10 ps to < 0.1 ps by exciting to a specific higher-lying excited state denoted here as S_n . Non-adiabatic transitions during internal conversion from S_n to the lowest-lying excited state, S_1 , allow momentum redistribution so that electronic energy is efficiently dumped into torsional modes. The excess kinetic energy in the torsional modes at early times allows the nuclei to move almost independently of the solvent environment and therefore undergo sub-100 fs torsional relaxation in a quasi-inertial manner. Exciting to another higher-lying state (S_m) does not have the same effect and the 'slow' picosecond reorganization is recovered allowing us to optically control the rate of conformational reorganization by selectively exciting to S_n (< 0.1 ps) or S_m (~ 10 ps).

We believe the findings shown here are general for a broad class of soft organic electronic molecular materials and suggest new optoelectronic applications for the future. Moreover, our results expose the fundamental rich physics of optical control of molecular conformation by demonstrating experimental evidence of ultrafast torsional reorganization.

Excited states of oligofluorenes

The absorption, photoluminescence and transient absorption (at 1 ps pump–probe delay) spectra of a penta-(9,9-dioctylfluorene) in

dilute toluene solution are shown in Fig. 1a. Figure 1b shows the calculated spectra (see Methods and Supplementary Information). As with similar conjugated oligomers and polymers, the lowest-lying excited states probed by these spectra are excitonic transitions with varying degrees of delocalization. The degree of delocalization, defined as the electron–hole separation, is depicted by 'Le' in the transition density matrix plots in Fig. 1d. Each plot depicts probabilities of an electron moving from one molecular position (horizontal axis) to another (vertical axis)^{22,23}. The plots show that the S_1 state is moderately delocalized (maximal distance between electron and hole is less than two fluorene units) whereas the higher-energy (two-photon allowed) S_n state is a very delocalized transition. At a similar energy, a one-photon-allowed S_m state is a highly localized benzene-like transition where both an electron and a hole are confined to a single phenyl ring. The absorption spectra of these three states are marked in Fig. 1a,b.

Electronic transitions in soft materials such as these couple strongly to intramolecular vibrations such as C=C stretching^{18,20}, giving rise to the structured vibronic peaks evident in the photoluminescence spectrum in Fig. 1a. The striking lack of mirror symmetry between the absorption and photoluminescence spectra is due to coupling of the electronic transition to torsions of individual fluorene units around the inter-monomer bond^{24,25}. These torsional modes have a pronounced effect on the spectroscopy of conjugated oligomers owing to a huge increase in torsional frequency when going from the ground to the excited state^{24,25}. Absorption of light projects the broad distribution of conformations of the oligomer (reflecting the shallow ground-state torsional potential) onto a steep excited-state potential. Relaxation narrows the distribution of torsional angles, leading to a global flattening of the molecules in the ensemble and the narrowed photoluminescence spectrum. This torsional relaxation occurs on the picosecond timescale and can therefore be resolved using transient absorption spectroscopy.

In this experiment, a sub-150 fs 3.18 eV pump pulse excites the samples in the S_1 absorption band creating S_1 excitons that are initially in the ground-state conformation, according to the

¹Cavendish Laboratory, University of Cambridge, J J Thomson Avenue, Cambridge CB3 0HE, UK, ²Theoretical Division, Group T-1/CINT Mail Stop B268, Los Alamos National Laboratory, Los Alamos, New Mexico 87545, USA, ³Department of Electrical Engineering and Computer Science and Research Laboratory of Electronics, Massachusetts Institute of Technology, Cambridge, Massachusetts 02139, USA, ⁴Center for Nano Science and Technology @Polimi, Istituto Italiano di Tecnologia, Via Pascoli 70/3, 20133 Milano, Italy, ⁵Department of Physics Politecnico di Milano, Piazza L. Da Vinci 32, 20133 Milano, Italy. *e-mail: jc414@cam.ac.uk

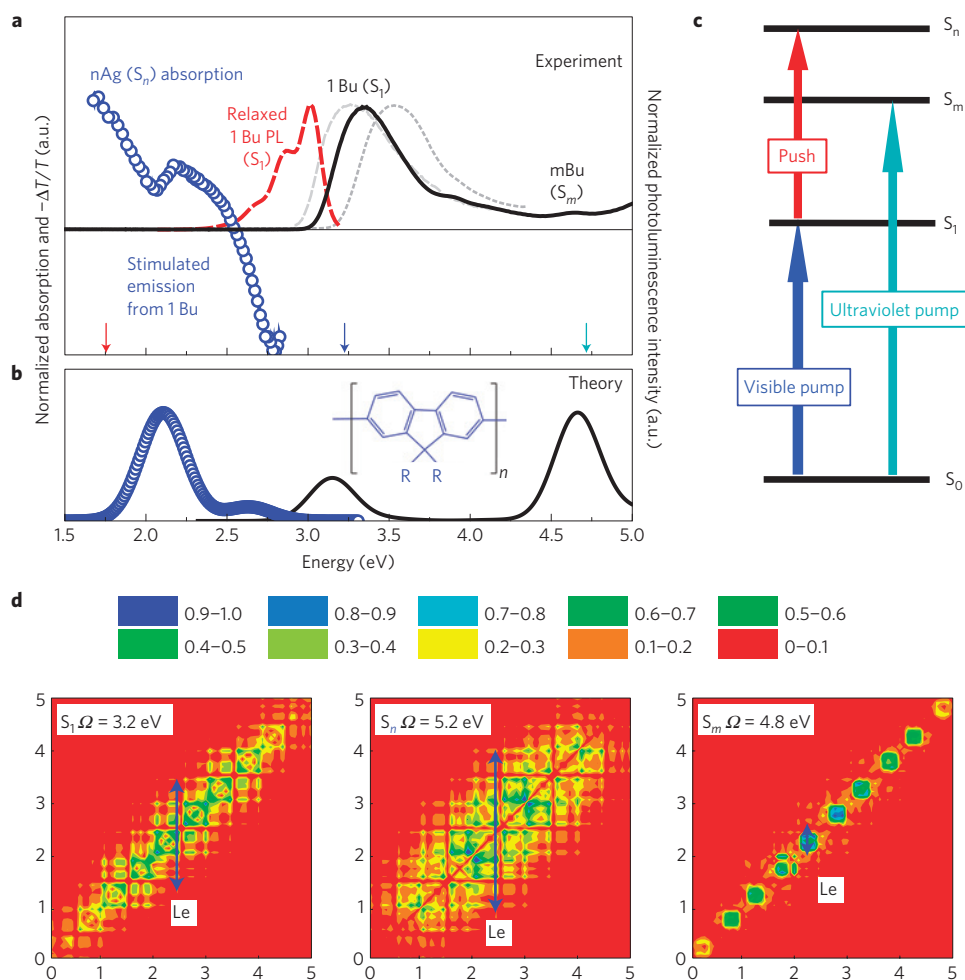


Figure 1 | Excited states of oligofluorenes in solution. **a**, Absorption (black solid), photoluminescence (red dashed) and transient absorption ($-\Delta T/T$, 1 ps delay; blue markers) spectra of the fluorene pentamer in toluene solution. Absorption spectra of the heptamer (grey dashed) and trimer (grey dotted) are shown for comparison. Coloured arrows denote approximate energies of the pump (blue, 3.18 eV), push (red, 1.59 eV) and ultraviolet-pump (cyan, 4.77 eV) pulses, as in part **c**. **b**, Calculated ground-state (black line) and excited-state (blue markers) absorption of the pentamer. Inset shows the chemical structure of the oligomers with $n = 3, 5$ or 7 (R is octyl for $n = 3, 5$ and hexyl for $n = 7$). **c**, Schematic (not to scale) showing the S_0, S_1, S_n and S_m states. S_1 and S_m are excited through one-photon transitions (blue and turquoise arrows), whereas S_n requires two-photon or sequential (pump+push) excitation, as marked (see text for details); the energies of the pump, ultraviolet pump and push are marked in **a**. **d**, Contour two-dimensional plots of transition density matrices of the excited states S_1, S_n and S_m for the fluorene pentamer. The axes label the repeat units of the oligomer. Each plot depicts probabilities of an electron moving from one molecular position (horizontal axis) to another (vertical axis) following electronic excitation according to the colour code. Le defines the exciton size (maximal distance between photoexcited electron and hole) on the polymer backbone.

Franck–Condon principle^{14,15}. A broadband white-light probe pulse transmitted through the excited sample at variable delays is dispersed in a spectrometer and measured. In this way, the excited-state absorption and stimulated emission of the oligomers can be measured as a function of wavelength and time, providing two-dimensional plots of $\Delta T/T$, such as those in Fig. 2. Here, the positive signal is assigned to stimulated emission from the singlet excitons, whereas the negative signal is assigned to singlet-exciton absorption^{26,27}. Within the first 40 ps, the spectra of the pentamer and heptamer shift to lower energies (redshift) whereas the singlet population does not decay significantly. The shift is demonstrated by the black arrow in Fig. 2 and is due to torsional relaxation as the molecular conformation changes from the ground-state geometry to the more planar excited-state geometry^{11,16–20,24,25,28,29}. The lack of sizable shift in the trimer is easily accounted for by considering the negligible reorganization energy following excitation at the very edge of the absorption spectrum, which corresponds to the planar molecules in the conformational distribution.

Ultrafast planarization

Following the dynamics at the red edge of the stimulated emission in Fig. 2 (470–480 nm) provides a handle with which to monitor torsional relaxation. These dynamics are shown by the red lines in Fig. 3a, demonstrating a slow rise as the molecules flatten in the pentamer and heptamer samples. Using a second pump pulse or push, which arrives a few picoseconds after the first 3.18 eV pump, we can excite the already excited molecules to the higher-lying S_n state depicted in Fig. 1. The time delay between the pump and push pulses is kept constant while the probe delay is altered, allowing us to monitor the effect of the push pulse on the stimulated emission dynamics.

The black lines with markers in Fig. 3a show the effect of the push. On arrival of the push, the stimulated emission is depleted. This is followed by a rapid increase in positive signal that appears as an ‘overshoot’ compared with the original slow torsional relaxation. As shown in Fig. 3a for the heptamer, the overshoot recovers to close to the final value in a manner that is independent of push timing. Figure 3b demonstrates that this

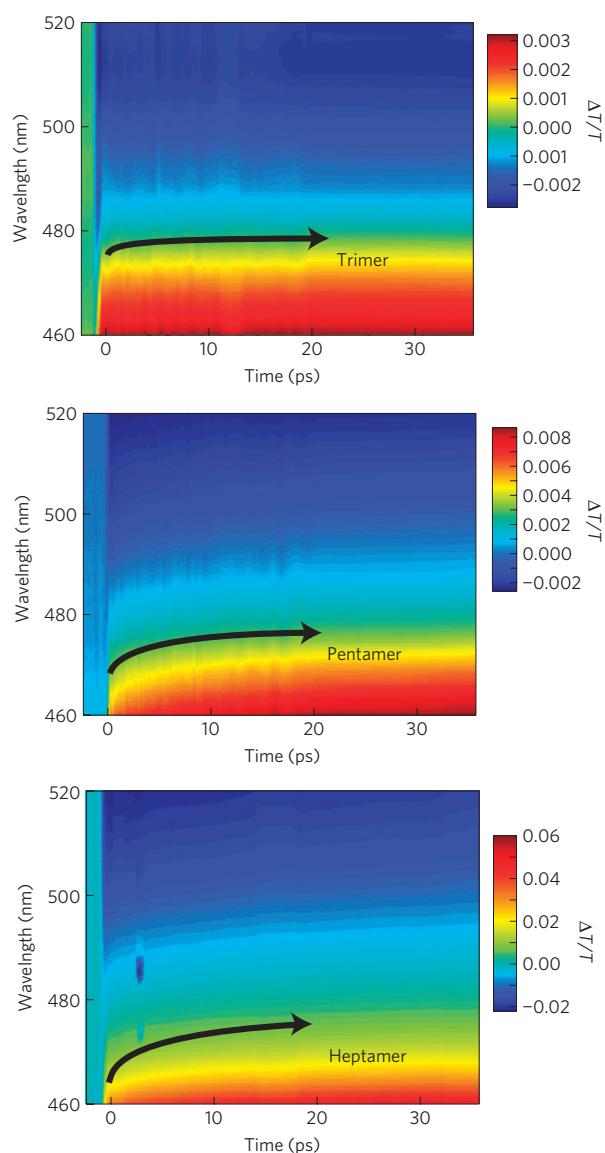


Figure 2 | Time-resolved torsional relaxation. Two-dimensional pump-probe spectra ($\Delta T(\tau, \lambda)/T$) of the trimer, pentamer and heptamer of fluorene in toluene solution. The pentamer and heptamer show a dynamic redshift, marked by the black arrow. The trimer shows a much smaller redshift (black arrow) as the excitation wavelength is at the bottom of the density of states (exciting already planar molecules).

overshoot is attributed to an ultrafast redshift of the spectrum. The slow redshift seen in the left-hand panel of Fig. 3b reproduces the data in Fig. 2 and demonstrates the slow torsional relaxation discussed above^{17,19}. The right panel, where the push arrives at 2.5 ps, shows the same spectral shift but on a much faster timescale; within 3 ps the full redshift has occurred. The push therefore induces an ultrafast planarization of the oligomers that leads to a redshift and a clear overshoot in the dynamics in Fig. 3a.

The push-induced redshift occurs within 150 fs, the temporal resolution of our instrument. To probe this with better resolution, we used sub-20 fs push and probe pulses, produced using the broadband output from two home-built non-collinear optical parametric amplifiers, compressed using a prism pair or chirped mirrors. The result is shown in Fig. 3c for the heptamer, which shows the arrival of the push pulse at 0 fs (arbitrarily set to zero) and the resulting overshoot. Fitting a mono-exponential rise provides

a time constant of ~ 60 fs for the S_n – S_1 internal conversion and accompanying torsional relaxation.

One final note on the data in Fig. 3a is that if the push arrives when the molecules are at or almost at the S_1 equilibrium geometry, the signal overshoots much further and then relaxes to the final value on a slower picosecond timescale. This is shown in the trimer (push at 4 ps) and in the heptamer when the push arrives at 18 ps in Fig. 3a.

To clarify the nature of the S_n state reached by the push, we probe the singlet absorption band at 820 nm and compare it with the stimulated emission dynamics measured at 480 nm (Fig. 4a,b). The effect of the push at 820 nm is much smaller than that at 480 nm because there is an additional push-induced absorption that overlaps with the stimulated emission at 480 nm. Excited-state absorption in this region is often attributed to charge (anion or cation) absorption³⁰ and recent work demonstrates similar behaviour in liquid⁴ and solid³ solutions of poly(9,9-dioctylfluorene). In the polymer case, the push-induced absorption was attributed to the formation of intrachain charge pairs that recombined rapidly^{3,31}. In the case of the oligomers studied here, it is unlikely that charge pairs are stabilized on a single chain. We therefore attribute the push-induced absorption to excited-state absorption from S_n . Calculations demonstrate that it is a highly delocalized state (Fig. 1d). We speculate that such a delocalized state is likely to gain significant charge-transfer character in the solvent environment, giving rise to an excited-state absorption similar to a charge pair. There is much debate as to the configuration of this excited state in polyfluorenes and other homo-polymers^{27,32,33} and our findings here could be direct evidence that the S_n state in oligofluorenes is a charge-transfer-type state and as such a precursor to fully charge-separated states³⁴.

In addition, Fig. 4c shows the stimulated emission when exciting to a highly localized Bu state known as S_m (Fig. 1) for the heptamer in cyclohexanone solution. Apart from a slight negative signal at early times, the same slow conformational relaxation seen when exciting S_1 (red line) is visible. Surprisingly, exciting to S_m does not result in ultrafast planarization, as seen when exciting S_n , despite the similar loss of electronic energy during internal conversion.

Non-adiabatic molecular dynamics: simulations

To rationalize these findings, we calculate the excited-state dynamics using the recently developed non-adiabatic excited-state molecular dynamics (NA-ESMD) framework^{35,36}. The NA-ESMD approach is described in the Methods and Supplementary Information. Briefly, a molecular dynamics with quantum transitions (MDQT) method allows us to model relaxation of photoexcited wave packets from the different excited states (S_n and S_m). The procedure is as follows. First, we run molecular dynamics at room temperature in the ground state to produce 500 different ground-state conformations of a fluorene pentamer. We then start the NA-ESMD simulations after populating the S_n (or S_m) state (500 times) allowing us to follow the internal conversion back to S_1 through multiple Born–Oppenheimer surfaces (for example, S_n is about 23 states above S_1) as the system passes non-adiabatic regions and state switches occur. The 500 trajectories, which were each started using a different molecular conformation, form a photoexcited wave packet that is propagated at room temperature for 400 fs. As a reference, we also carry out simulations of the Born–Oppenheimer dynamics of the ground state, S_0 , and the first excited state, S_1 , starting from the same initial conditions. Figure 5 shows the main result of our modelling (detailed analysis of the computational results is given in the Supplementary Information). Figure 5a shows the S_1 population as a function of time and demonstrates that the photoexcited wave packet placed in S_n undergoes internal conversion ($S_n \rightarrow S_1$) within 100 fs (that is, $\sim 75\%$ of the trajectories end up on the S_1 potential-energy surface

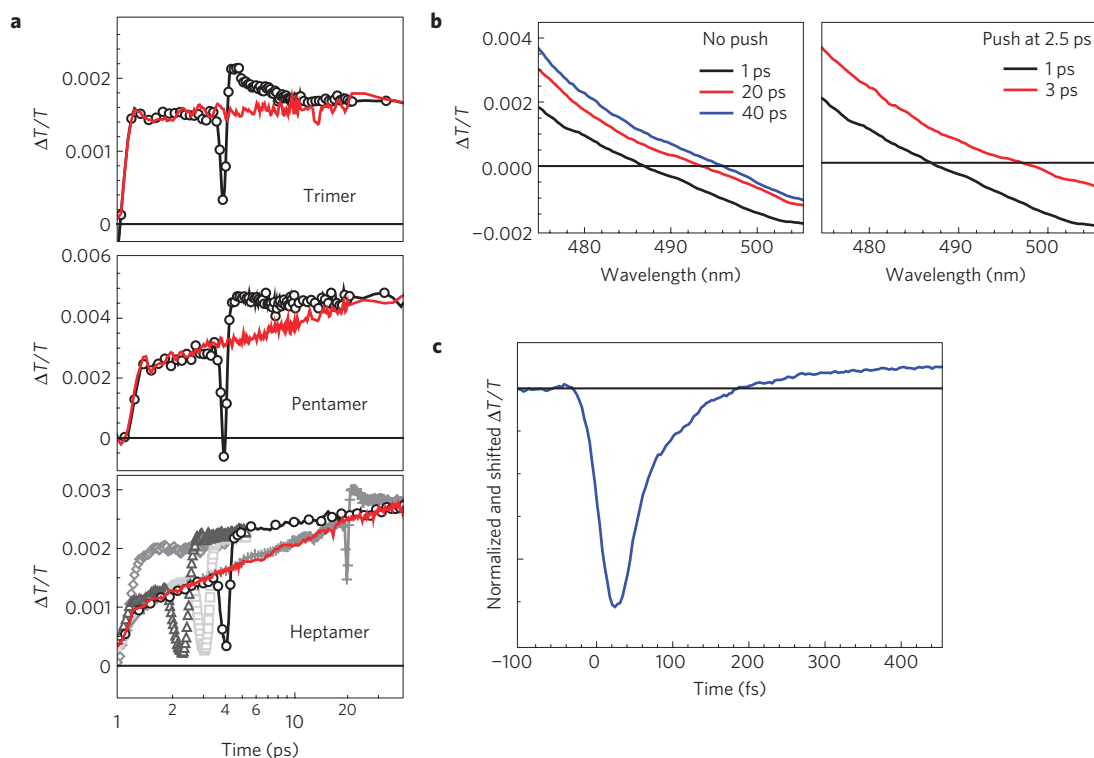


Figure 3 | Experimental observation of ultrafast planarization. **a**, Pump-probe (red lines) and pump-push-probe (markers) dynamics of the trimer, pentamer and heptamer in solution. The push arrives at 4 ps for the trimer and pentamer and at a variety of times for the heptamer (100 fs, diamonds; 1.2 ps, triangles; 2 ps, squares; 3.2 ps, circles; 18 ps crosses). **b**, Pump-probe (left) and pump-push-probe (right) spectra at the zero-crossing region for the pentamer. Note the slow redshift in the pentamer pump-probe spectra. The push (arriving at 2.5 ps) causes an immediate redshift. **c**, Pump-push-probe dynamics at 480 nm of the heptamer in solution, measured with ≤ 20 fs temporal resolution, showing only the arrival of the push (push arrival arbitrarily set to 0 fs) and the subsequent recovery, which has a time constant of ~ 60 fs.

(PES) within this timescale). This is much faster than the internal conversion from S_m , which is also shown. Figure 5b shows that the ultrafast internal conversion from S_n to S_1 is accompanied by a local flattening of the molecule.

This ultrafast flattening can be described in the context of previous work^{37,38} where at each surface hop (non-adiabatic transition), the velocity of the wave packet is re-scaled in the direction of the non-adiabatic coupling vector. Each non-adiabatic transition therefore allows donation of electronic energy into the torsional modes. Owing to the many non-adiabatic transitions that occur between S_n and S_1 , momentum (and therefore kinetic energy) is donated to the torsional motion causing rapid planarization. The nuclei effectively gain such high kinetic energy that flattening occurs within 100 fs.

The resulting near-zero average torsional angle in Fig. 5b appears as arithmetic averaging of a minor portion of trajectories that ‘overshoot’ by flipping to a negative angle. Both the ultrafast internal conversion and the planarization are consistent with experimental findings in Figs 3 and 4 and will be discussed further below. We note that, as expected, on the timescale of the calculation (400 fs), the ground-state S_0 torsional angle barely varies around its equilibrium value whereas the S_1 angular distribution reduces by $\sim 5^\circ$ over 400 fs. Interestingly, the trajectory from S_m shows little change in torsional angle over the first 400 fs.

Discussion

The surprising finding that the non-adiabatic dynamics starting from S_n quickly flattens the molecule locally, leading to the ultrafast conformational relaxation we have observed, is worthy of fuller discussion. We start by considering the reason for the ultrafast electronic part of the internal conversion between S_n and S_1 ,

which effectively reduces the energy of the electronic state by ~ 1.5 eV within 100 fs.

That internal conversion occurs on such a short timescale is not obvious (for example, internal conversion from S_m is simulated to be significantly slower). Its speed here is aided by several factors, as discussed in greater detail in the Supplementary Information. First, the underlying non-adiabatic dynamics involve transitions between many intermediate states that lie between S_n and S_1 (ref. 23) and are similarly delocalized to S_n . The similarity results in large non-adiabatic couplings between states, promoting fast down-energy transitions. Second, PESs of delocalized excitons (particularly S_n) are relatively steep along not only the torsional degree of freedom (Supplementary Information), but also along the high-frequency C=C stretching motions, which lead to a quinoid structure. Consequently, the wave packet gains substantial velocity along these two strongly coupled vibrational coordinates, transferring an excess of the electronic energy into vibrations. The slower internal conversion from the S_m state occurs because the relaxation process cannot use the efficient non-adiabatic pathway followed by S_n owing to reduced non-adiabatic coupling between localized (S_m) and delocalized (S_1 and other) states. As a result, the internal conversion from S_m is much slower compared with that from S_n .

We have explained the ultrafast internal conversion from S_n to S_1 but have not yet fully accounted for the ultrafast planarization that accompanies it. Although the S_n PES is steep in the torsional direction, considering only adiabatic relaxation along this coordinate is not enough to describe the increase in torsional relaxation timescale that we observe.

We note that the ultrafast planarization is highly analogous to the work on solvation dynamics^{39–41}, where solvent reorganization following photoexcitation of a solute is ultrafast owing to inertial

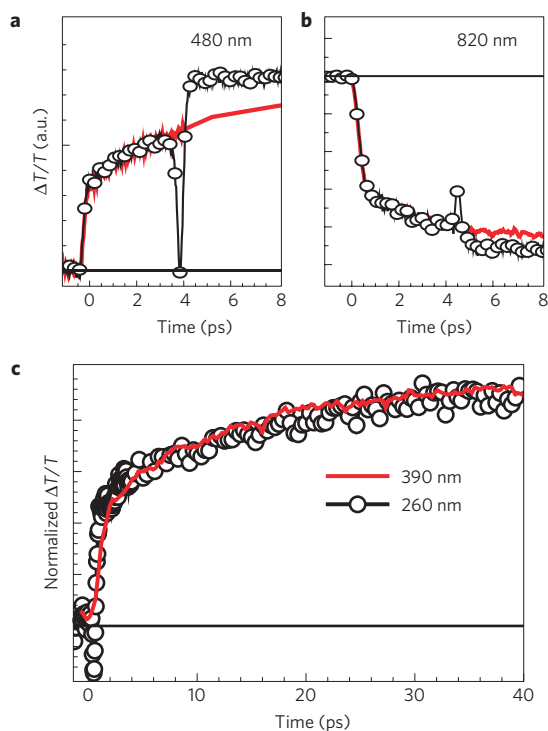


Figure 4 | Nature of S_n and reorganization dynamics from S_m .

a,b, Pump-probe (red lines) and pump-push-probe (black lines with markers) dynamics measured in the heptamer in solution at 480 nm (**a**) and 820 nm (**b**) probe wavelength. **c**, Pump-probe dynamics exciting at 390 nm (3.18 eV; directly to S_1 , red lines) and exciting at 260 nm (4.77 eV; directly to S_m , black lines with markers). Measured on the heptamer in toluene (390 nm) or cyclohexanone (266 nm) with a probe wavelength of 480 nm in both cases.

motions of the solvent molecules. These initial motions are highly local such that each solvent molecule moves independently from the others in a manner determined by pairwise interactions with the solute. The analogy here is clear; the ultrafast torsional motion occurs on similar timescales, and locally flattens the molecule. Indeed, subpicosecond torsional reorganization has previously been observed in 9,9'-bianthryl in solution and described as inertial torsional relaxation^{42,43}. For such fast torsional motion to occur, significant energy must be dumped into the torsional modes, allowing the nuclei to move quasi-independently from the solvent environment. The mechanism that converts the excess electronic energy acquired from the push into kinetic energy of the nuclei is the many non-adiabatic transitions that occur during internal conversion (mentioned above).

Following previous work^{37,38}, each non-adiabatic transition allows donation of electronic energy into the torsional modes. Owing to the many non-adiabatic transitions that occur between S_n and S_1 , the nuclei effectively gain such high kinetic energy that they move quasi-independently of the solvent in an almost frictionless manner. Their speed is much higher than that allowed on the S_1 PES by the local potential gradient during adiabatic adjustment. As a consequence, flattening occurs within 100 fs.

We note that although the initial torsional relaxation occurs within 100 fs, it is not truly 'free' motion. Figure 5b shows that the initial torsional relaxation is linear in time, rather than quadratic, as expected for free motion caused by a force. This demonstrates that 'friction' (dissipation of energy through coupling to solvent modes for example) still plays a role in the initial relaxation pathway. On the sub-100 fs timescale the non-adiabatic energy influx overcomes this friction prompting large torsional reorganization. Once the

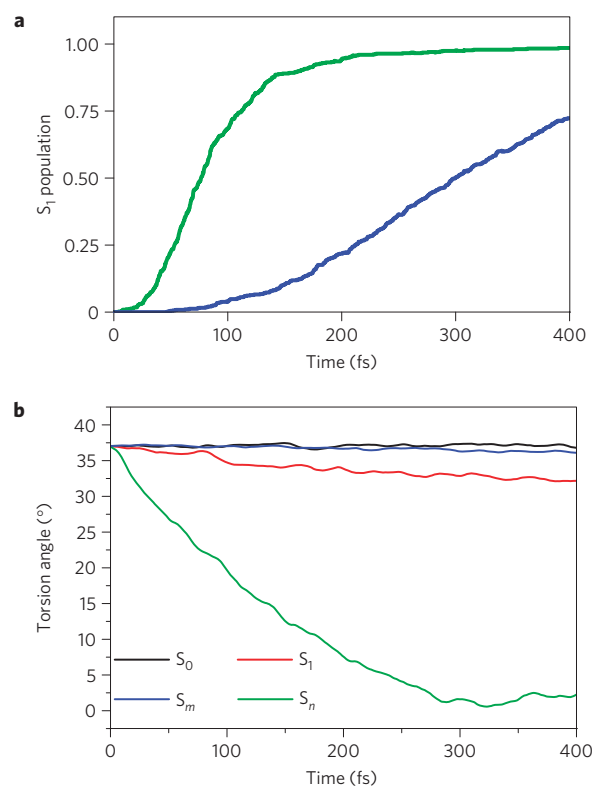


Figure 5 | Photoinduced dynamics simulations for S_0 , S_1 , S_n and S_m states, averaged over 500 trajectories to obtain statistical averages.

a, An increase of population of the S_1 state during non-adiabatic dynamics starting from S_m and S_n states. Population of S_n quickly drops to the S_1 state within ~ 100 fs, showing ultrafast non-adiabatic relaxation, whereas the S_m state relaxes on a much slower timescale (>400 fs). **b**, Variation of the minimum torsion angle between fluorene units on each molecule averaged over 500 molecules (snapshots) taken along the trajectory. The curves for S_0 and S_m are flat, showing no time dependence; the S_1 state shows weak torsional relaxation over the first 400 fs, whereas vibrational relaxation following S_n excitation results in a local planarization of the molecule within the first 100 fs of dynamics.

non-adiabatic energy influx is over, the anharmonic coupling (friction) presumably regains control, slowing down the motion by conversion of energy from torsional degrees of freedom into other vibrational and solvent modes. This effectively damps the torsional motion on longer timescales and prevents the molecules from 'overshooting' past the S_1 minimum. The fact that the torsional motion can overshoot is seen in Fig. 3a most clearly for the trimer. When the excited molecules are already near the S_1 PES minimum, the push-induced inertial behaviour of the nuclei causes them to become more planar than the S_1 equilibrium geometry. The subsequent 'twisting' of the molecule back to the S_1 PES equilibrium geometry (at 20° inter-monomer angle) occurs on a much slower picosecond timescale. We think that it is only the 'friction' from anharmonic coupling that prevents a similar over-planarization from occurring when the molecules start off far from equilibrium.

The lack of ultrafast planarization when exciting to S_m is due partly to the flat PES of the S_m state, but more specifically to the fewer non-adiabatic transitions that occur during internal conversion between S_m and S_1 . We note that the flatness of the PES and the lack of non-adiabatic transitions are actually related as steep PES gradients generally lead to large components of the non-adiabatic coupling vector along the given direction (Supplementary Information). The lack of non-adiabatic crossings means that the wave packet arrives at S_1 with little kinetic energy

in the torsional direction. Energy instead is slowly released through damped torsional relaxation in the S_1 PES.

Conclusions

We report here a sub-100 fs conformational reorganization in oligofluorenes and propose that it is analogous to 'inertial solvent reorganization' described in the 1990s (refs 39–41). To put these findings into context, we compare them to one of the best-known examples of conformational reorganization in molecular systems, the primary step in vision (*cis*–*trans* isomerization in rhodopsin and bacteriorhodopsin^{44–46}). In these systems, photoisomerization involves one electronic curve crossing (that is, a non-adiabatic transition) between the S_1 and S_0 states that occurs within 200 fs. However, most of the conformational change occurs adiabatically on the ground-state PES with a slower picosecond timescale, despite the ultrafast S_1 to S_0 internal conversion^{12,21}. The *cis*–*trans* conformational reorganization in rhodopsin can therefore be directly compared to the adiabatic torsional relaxation of oligofluorenes in the S_1 state. The difference in this work is that we can speed up the conformational reorganization by over two orders of magnitude using a 'kick' from the push pulse, making it substantially faster than the rhodopsin benchmark.

We note that subpicosecond (~ 800 fs) torsional relaxation has previously been demonstrated in bianthryl molecules and attributed to inertial torsional relaxation^{42,43}. However, this occurred in the S_1 excited state and the force driving the reorganization was charge transfer. We propose that in the oligofluorenes studied here, it is the many non-adiabatic surface hops during internal conversion between S_n and S_1 that drives the conformational reorganization, causing it to occur in under 100 fs. Essentially, the non-adiabatic surface hops dump energy into the torsional degrees of freedom allowing the molecular rings in the excited fluorene oligomer to rotate towards equilibrium almost independently of the environment. This is a sort of incoherent light control that allows one to decide in advance the path in configurational space, so that the molecule either slowly planarizes (after S_1 and S_m excitation) or suddenly locks into the flat geometry (after S_n excitation). As a matter of fact, we can speed up large torsional reorganization well over 100 times in the same environment. This rules out classical over-damping caused by the solvent cage interaction. We speculate that ultrafast torsional relaxation may be exploited for nonlinear optical processes in organic systems. The strong Stokes shift associated with the ring conformational motion for example suggests exploitation of this phenomenon for optical switching, as re-excitation with a push pulse leads to a sudden shift of the emission wavelength.

Methods

Experimental. Oligofluorenes were purchased from American Dye Source and used as received. They were dissolved in toluene (for most experiments), or cyclohexanone (for experiments requiring ultraviolet (260 nm) excitation as cyclohexanone does not strongly absorb at 260 nm, whereas toluene does; both from Aldrich) in air to form dilute solutions. Photoluminescence measurements were carried out using a Cary Eclipse spectrophotometer. Absorbance measurements were carried out on a Hewlett-Packard ultraviolet–visible spectrometer in ambient conditions.

Conventional pump–probe transient absorption spectroscopy, as outlined previously^{5,26}, was carried out on the solution samples. In this experiment, pump pulses at 3.18 eV (or 4.77 eV), the second (or third) harmonic of the output of a CLARK Ti:sapphire regenerative amplifier with a repetition rate of 1 kHz and a pulse length of 150 fs, are focused to a ~ 200 μm diameter spot, giving an excitation energy density between 1 and 0.01 mJ cm⁻². The probe beam is a white-light continuum 1.22–2.76 eV (450–1,100 nm), generated by focusing the CLARK amplifier output onto a sapphire plate. Pump and probe pulses, delayed with respect to each other by a computer-controlled delay line with ~ 5 fs accuracy, are spatially overlapped on the sample. The probe is then dispersed in a prism spectrometer and detected using a Stresing optical multi-channel analyser with fast data acquisition. The pump was mechanically chopped at 500 Hz allowing on-the-fly measurements of the pump-induced change in transmission ($\Delta T(\tau, \lambda)/T$) as a function of pump–probe delay (τ) and probe wavelength (λ).

Using a second 'pump' pulse or push pulse that arrives a few picoseconds after the pump, as outlined previously^{5,31}, we re-excite the already excited samples. We use the Ti:sapphire laser fundamental at 1.57 eV for the push pulse as it excites directly into the S_1 absorption band. The push and probe maintain the 1 kHz repetition rate of the laser, whereas the pump is mechanically chopped at 500 Hz. For each experiment, the pump and push delay is fixed while the relative probe delay is scanned, as in the conventional pump–probe experiment. The effect of the push pulse on the pump–probe spectrum is determined by comparing the pump–probe and the pump–push–probe dynamics, as in Fig. 3.

For the short-pulse measurements with ≤ 20 fs temporal resolution shown in Fig. 4c, pumping was from the second harmonic of the Ti:sapphire laser at 3.18 eV (~ 150 fs) as above. However, the push and probe were generated using two home-built non-collinear optical parametric amplifiers (centred at 750 nm and 490 nm respectively) and compressed using either chirped mirrors or a prism pair as outlined previously⁴⁷. After the sample, the probe beam was filtered with a 470 ± 10 nm interference filter and measured using a photodiode. A lock-in amplifier, locked to the pump, was used to determine ΔT , which was then normalized for the transmission to determine $\Delta T/T$ both with and without the push.

Theoretical. To model non-adiabatic excited-state dynamics in a photoexcited polyfluorene pentamer and rationalize experimentally observed relaxation timescales and concomitant conformational motions, we use the recently developed non-adiabatic excited-state molecular dynamics (NA-ESMD) code. The NA-ESMD approach combines the fewest-switches surface-hopping algorithm, as it is used in the MDQT method³⁸, with the 'on the fly' calculation of the electronic energies, gradients and non-adiabatic coupling vectors for the excited states. The configuration interaction singles (CIS) combined with the Austin Model 1 (AM1) semi-empirical model Hamiltonian serves as a numerically efficient technique for computing excited states in large systems. A detailed description of the NA-ESMD implementation can be found elsewhere^{35,36}. The MDQT treats the electronic degrees of freedom quantum mechanically, whereas the motion of the nuclei is treated classically. The nuclei of each trajectory are evolved on a single adiabatic PES following the classical Langevin equation of motion. The probability for a quantum transition from the present excited state to any other excited state depends on the strength of the non-adiabatic couplings between excited states calculated at each integration step along the trajectory. An appropriate statistical sampling is required to compute detailed photoinduced wave-packet evolution (such as branching and relaxation timescales). Consequently, a 'swarm' (typically a few hundred) of classical trajectories with initial conditions selected should be propagated along different excited-state PESs. Such treatment of non-adiabatic effects allows one to preserve the detailed balance conditions and to account for trajectory branching.

We start with the ground-state geometry optimization at the AM1 level and calculate ground- and excited-state absorption spectra shown in Fig. 1 using the AM1-CIS approach. Two-dimensional plots of the transition density matrices of the essential excited states are shown in Fig. 1 as well. We further continue with the AM1 ground-state molecular dynamics simulations of 400-ps-long Born–Oppenheimer trajectories at 300 K with the time step $\Delta t = 0.5$ fs. The system was heated and allowed to equilibrate to a final temperature of 300 K during the first 20 ps. The Langevin thermostat⁴⁸ was used to keep the temperature constant with a friction coefficient $\zeta = 2.0$ ps⁻¹. The rest of the trajectory was used to collect a set of initial positions and momenta for the subsequent simulations of the excited states. Configurations were sampled for a total of 500 configurations. Excited-state dynamics trajectories were started from these initial configurations after photoexcitation. We considered several cases. Dynamics of the ground state S_0 and the first excited state S_1 , where the nuclei are propagated on a single Born–Oppenheimer PES, serve as reference points. Modelling of photoexcited dynamics after populating the highly excited S_n and S_m states targets the interband relaxation through multiple Born–Oppenheimer surfaces as the system passes non-adiabatic regions and state switches occur while the system relaxes back to the S_1 state. Fifty lowest excited states have been calculated for every snapshot to determine energetic positions of S_n and S_m states. We further use the NA-ESMD code to propagate all trajectories for 500 fs at 300 K. A classical step $\Delta t = 0.1$ fs and $N_q = 3$ quantum steps were used in all simulations.

Received 28 July 2011; accepted 14 December 2011;
published online 5 February 2012

References

- Clark, J. & Lanzani, G. Organic photonics for communications. *Nature Photon.* **4**, 438–446 (2010).
- Yap, B. K., Xia, R. D., Campoy-Quiles, M., Stavrinou, P. N. & Bradley, D. D. C. Simultaneous optimization of charge-carrier mobility and optical gain in semiconducting polymer films. *Nature Mater.* **7**, 376–380 (2008).
- Virgili, T., Marinotto, D., Manzoni, C., Cerullo, G. & Lanzani, G. Ultrafast intrachain photoexcitation of polymeric semiconductors. *Phys. Rev. Lett.* **94**, 117402 (2005).
- Vishnubhatla, K. C., Clark, J., Lanzani, G., Ramponi, R., Osellame, R. & Virgili, T. Ultrafast optofluidic gain switch based on conjugated polymer in femtosecond laser fabricated microchannels. *Appl. Phys. Lett.* **94**, 041123 (2009).

5. Virgili, T. *et al.* Ultrafast optical gain switch in organic photonic devices. *J. Mater. Chem.* **20**, 519–523 (2010).
6. Kabra, D., Lu, L. P., Song, M. H., Snaith, H. J. & Friend, R. H. Efficient single-layer polymer light-emitting diodes. *Adv. Mater.* **22**, 3194–3198 (2010).
7. Barlow, I. A., Kreouzis, T. & Lidzey, D. G. High-speed electroluminescence modulation of a conjugated-polymer light emitting diode. *Appl. Phys. Lett.* **94**, 243301 (2009).
8. McNeill, C. R. & Greenham, N. C. Conjugated-polymer blends for optoelectronics. *Adv. Mater.* **21**, 3840–3850 (2009).
9. Clarke, T. M. & Durrant, J. R. Charge photogeneration in organic solar cells. *Chem. Rev.* **110**, 6736–6767 (2010).
10. Sakanoue, T. & Sirringhaus, H. Band-like temperature dependence of mobility in a solution-processed organic semiconductor. *Nature Mater.* **9**, 736–740 (2010).
11. Spano, F. C. & Silvestri, L. Multiple mode exciton-vibrational coupling in h-aggregates: synergistic enhancement of the quantum yield. *J. Chem. Phys.* **132**, 094704 (2010).
12. Kukura, P., McCamant, D. W., Yoon, S., Wandschneider, D. B. & Mathies, R. A. Structural observation of the primary isomerization in vision with femtosecond-stimulated Raman. *Science* **310**, 1006–1009 (2005).
13. Tamai, N. & Miyasaka, H. Ultrafast dynamics of photochromic systems. *Chem. Rev.* **100**, 1875–1890 (2000).
14. Franck, J. Elementary processes of photochemical reactions. *Trans. Faraday Soc.* **21**, 536–542 (1926).
15. Condon, E. A theory of intensity distribution in band systems. *Phys. Rev.* **28**, 1182–1201 (1926).
16. Lanzani, G., Nisoli, M., DeSilvestri, S. & Tubino, R. Femtosecond vibrational and torsional energy redistribution in photoexcited oligothiophenes. *Chem. Phys. Lett.* **251**, 339–345 (1996).
17. Hintschich, S. I., Dias, F. B. & Monkman, A. P. Dynamics of conformational relaxation in photoexcited oligofluorenes and polyfluorene. *Phys. Rev. B* **74**, 045210 (2006).
18. Justino, L. L. G. *et al.* Conformational studies of poly(9,9-dialkylfluorene)s in solution using NMR spectroscopy and density functional theory calculations. *J. Phys. Chem. B* **113**, 11808–11821 (2009).
19. Chen, H. L. Excited-state backbone twisting of polyfluorene as detected from photothermal after-effects. *J. Phys. Chem. B* **113**, 8527–8531 (2009).
20. Parkinson, P., Muller, C., Stingelin, N., Johnston, M. B. & Herz, L. M. Role of ultrafast torsional relaxation in the emission from polythiophene aggregates. *J. Phys. Chem. Lett.* **1**, 2788–2792 (2010).
21. Prokhorenko, V. I. Coherent control of retinal isomerization in bacteriorhodopsin. *Science* **313**, 1257–1261 (2006).
22. Tretiak, S., Saxena, A., Martin, R. L. & Bishop, A. R. Conformational dynamics of photoexcited conjugated molecules. *Phys. Rev. Lett.* **89**, 097407 (2002).
23. Wu, C., Malinin, S. V., Tretiak, S. & Chernyak, V. Y. Exciton scattering and localization in branched dendrimeric structures. *Nature Phys.* **2**, 631–635 (2006).
24. Karabunarliev, S., Bittner, E. R. & Baumgarten, M. Franck-Condon spectra and electron-libration coupling in para-polyphenyls. *J. Chem. Phys.* **114**, 5863–5870 (2001).
25. Karabunarliev, S., Baumgarten, M., Bittner, E. R. & Mullen, K. Rigorous Franck-Condon absorption and emission spectra of conjugated oligomers from quantum chemistry. *J. Chem. Phys.* **113**, 11372–11381 (2000).
26. Clark, J. *et al.* Blue polymer optical fiber amplifiers based on conjugated fluorene oligomers. *J. Nanophoton.* **2**, 023504 (2008).
27. Hayes, S. C. & Silva, C. Analysis of the excited-state absorption spectral bandshape of oligofluorenes. *J. Chem. Phys.* **132**, 214510 (2010).
28. Franco, I. & Tretiak, S. Electron-vibrational dynamics of photoexcited polyfluorenes. *J. Am. Chem. Soc.* **126**, 12130–12140 (2004).
29. Westenhoff, S. *et al.* Anomalous energy transfer dynamics due to torsional relaxation in a conjugated polymer. *Phys. Rev. Lett.* **97**, 166804 (2006).
30. Fratiloiu, S. *et al.* Electronic structure and optical properties of charged oligofluorenes studied by VIS/NIR spectroscopy and time-dependent density functional theory. *J. Phys. Chem. B* **110**, 5984–5993 (2006).
31. Virgili, T., Marinotto, D., Lanzani, G. & Bradley, D. D. C. Ultrafast resonant optical switching in isolated polyfluorenes chains. *Appl. Phys. Lett.* **86**, 091113 (2005).
32. Tong, M., Sheng, C. X. & Vardeny, Z. V. Nonlinear optical spectroscopy of excited states in polyfluorene. *Phys. Rev. B* **75**, 125207 (2007).
33. Zhang, X. P., Xia, Y. J. & Friend, R. H. Multiphoton excited photoconductivity in polyfluorene. *Phys. Rev. B* **75**, 245128 (2007).
34. Kohler, A. *et al.* Charge separation in localized and delocalized electronic states in polymeric semiconductors. *Nature* **392**, 903–906 (1998).
35. Nelson, T., Fernandez-Alberti, S., Chernyak, V., Roitberg, A. E. & Tretiak, S. Nonadiabatic excited-state molecular dynamics modeling of photoinduced dynamics in conjugated molecules. *J. Phys. Chem. B* **115**, 5402–5414 (2011).
36. Fernandez-Alberti, S., Kleiman, V. D., Tretiak, S. & Roitberg, A. E. Unidirectional energy transfer in conjugated molecules: The crucial role of high-frequency C≡C bonds. *J. Phys. Chem. Lett.* **1**, 2699–2704 (2010).
37. Tully, J. C. & Preston, R. K. Trajectory surface hopping approach to nonadiabatic molecular collisions—reaction of H⁺ with D₂. *J. Chem. Phys.* **55**, 562–572 (1971).
38. Tully, J. C. Molecular-dynamics with electronic-transitions. *J. Chem. Phys.* **93**, 1061–1071 (1990).
39. Rosenthal, S. J., Xie, X. & Fleming, G. R. Femtosecond solvation dynamics in acetonitrile: Observation of the inertial contribution to the solvent response. *J. Chem. Phys.* **95**, 4715–4718 (1991).
40. Stratt, M. R. & Cho, M. The short-time dynamics of solvation. *J. Chem. Phys.* **9**, 6700–6708 (1994).
41. Jimenez, R., Fleming, G. R., Kumar, P. V. & Maroncelli, M. Femtosecond solvation dynamics of water. *Nature* **369**, 471–473 (1994).
42. Elich, K., Kitazawa, M., Okada, T. & Wortmann, R. Effect of s-1 torsional dynamics on the time-resolved fluorescence spectra of 9,9'-bianthryl in solution. *J. Phys. Chem. A* **101**, 2010–2015 (1997).
43. Jurczok, M., Plaza, P., Martin, M. M., Meyer, Y. H. & Rettig, W. Excited state relaxation paths in 9,9'-bianthryl and 9-carbazolyl-anthracene: A sub-ps transient absorption study. *Chem. Phys.* **253**, 339–349 (2000).
44. Miller, R. J. D. 'Making the molecular movie': First frames. *Acta Crystallogr. A* **66**, 137–156 (2010).
45. Shoenlein, R. W., Peteanu, L. A., Mathies, R. A. & Shank, C. V. The 1st step in vision—femtosecond isomerization of rhodopsin. *Science* **254**, 412–415 (1991).
46. Polli, D. *et al.* Conical intersection dynamics of the primary photoisomerization event in vision. *Nature* **467**, 440–U88 (2010).
47. Brida, D. *et al.* Few-optical-cycle pulses tunable from the visible to the mid-infrared by optical parametric amplifiers. *J. Opt.* **12**, 013001 (2010).
48. Allen, M. P. & Tildesley, D. J. *Computer Simulation of Liquids* (Oxford Univ. Press, 1990).

Acknowledgements

We thank S. Fernandez-Alberti for stimulating discussions and for help with the code for the non-adiabatic simulations. J.C. acknowledges the Royal Society for a Dorothy Hodgkin Fellowship. We also acknowledge support of the Center for Integrated Nanotechnology (CINT), the Center for Nonlinear Studies (CNLS) and the LDRD programme at Los Alamos National Laboratory, operated by Los Alamos National Security, LLC, for the National Nuclear Security Administration of the US Department of Energy under contract DE-AC52-06NA25396, as well as the European Union for financial support through FP6-026365.

Author contributions

J.C. and G.L. devised the experiments, J.C. and G.C. carried out the experiments and J.C. and G.L. analysed the data. S.T. and T.N. carried out the calculations that were devised by S.T., J.C., G.L., S.T. and T.N. wrote the paper.

Additional information

The authors declare no competing financial interests. Supplementary information accompanies this paper on www.nature.com/naturephysics. Reprints and permissions information is available online at www.nature.com/reprints. Correspondence and requests for materials should be addressed to J.C.